High energy density aluminum/oxygen cell

E.J. Rudd and D.W. Gibbons
ELTECH Research Corporation, Fairport Harbor, OH 44077 (USA)

Abstract

An alternative to a secondary battery as the power source for vehicle propulsion is a fuel cell, an example of which is the metal/air cell using metals such as aluminum, zinc, or iron. Aluminum is a particularly attractive candidate, with high energy and power densities, environmentally acceptable and having a large, established industrial base for production and distribution. An aluminum/oxygen system is currently under development for a prototype unmanned, undersea vehicle (UUV) for the US navy and recent work has focussed upon low corrosion aluminum alloys, and an electrolyte management system for processing the by-products of the energy-producing reactions. This paper summarizes the progress made in both areas. Anode materials capable of providing high utilization factors over current densities ranging from 5 to 150 mA/cm^2 have been identified, such materials being essential to realize mission life for the UUV. With respect to the electrolyte management system, a filter/precipitator unit has been successfully operated for over 250 h in a large scale, half-cell system.

Introduction

An alternative to a secondary battery as the power source in a vehicle is a fuel cell. It has been shown that metals such as aluminum, zinc, lithium and iron may be used as a 'fuel' in the fuel cell or metal/air battery. Aluminum is a particularly attractive candidate. The metal has both high energy and power densities, it is environmentally acceptable (as are the products of the cell reaction), it is easy to handle and has a large, industrial base for production and distribution.

The chemistry that is involved in the aluminum/air cell is shown by the following equations:

(i) overall cell reaction

$$Al + KOH + 3/4O_2 + 3/2H_2O \longrightarrow KAl(OH)_4 \quad (1)$$

(ii) anode reaction

$$Al + KOH + 3OH^- \longrightarrow KAl(OH)_4 + 3e^- \quad (1a)$$

(iii) cathode reaction

$$3/4O_2 + 3/2H_2O + 3e^- \longrightarrow 3OH^- \quad (1b)$$

(iv) corrosion reaction

$$Al + KOH + 3H_2O \longrightarrow 3/2H_2\uparrow + KAl(OH)_4 \quad (2)$$

0378-7753/94/$07.00
SSDI 0378-7753(93)01776-E

(v) crystallization reaction

$$KAl(OH)_4 \longrightarrow KOH + Al(OH)_3 \downarrow \quad (3)$$

In operation, aluminum is dissolved (eqn. (1)) forming a soluble aluminate species and consuming the alkali metal hydroxide in the electrolyte. A corrosion reaction also occurs in the aqueous electrolyte, again forming the soluble aluminate together with hydrogen gas (eqn. (2)). This corrosion reaction is a coulombic inefficiency and, therefore, must be minimized. As the battery operates, the conductivity of the electrolyte decreases until precipitation or crystallization of aluminum trihydroxide occurs (eqn. (3)), replenishing 'free' hydroxide. Thus, a 'steady-state' condition may be achieved with respect to electrolyte composition and conductivity, at which time the electrolyte will contain crystals of aluminum trihydroxide. As well be discussed later, controlling the electrolyte composition is very important.

The reaction at the cathode is the electroreduction of oxygen, which can only be sustained at practical rates by using a gas-diffusion electrode. A three-phase boundary between the catalyst, electrolyte and reactant oxygen must be established and this demands a unique electrode structure. It is known that the presence of carbon dioxide in the air feed stream to the cathode can lead to loss of performance, due probably to precipitation of alkali metal carbonates within the structure of the electrode. Therefore, the battery system must include a method to reduce the levels of carbon dioxide in the air feed stream, or ideally to remove it entirely. For a power source in an underwater vehicle, the fuel is necessarily oxygen, probably cryogenic oxygen, and removal of carbon dioxide is not required.

Aluminum cannot be electrodeposited from aqueous solutions, so that the aluminum/air battery is not a true secondary battery. The anode must be replaced mechanically, requiring novel features in the cell design, but offering relatively rapid refuelability.

The aluminum/air battery is, therefore, a multicomponent system (Fig. 1) and programs to develop this technology have necessarily focussed upon:

- the electrodes
- the electrolyte management system, i.e., the separation of crystals of aluminum trihydroxide from the electrolyte and control of the composition and conductivity of that electrolyte
- cell design to allow replacement of the anode material
- the auxiliary system, including a heat-exchange unit, safe handling and/or disposal of hydrogen gas and control of carbon dioxide in the air feed stream

This paper will provide a brief review and summarize the recent progress made in the first two areas, the electrodes and the electrolyte management system.

Electrodes

Development of aluminum alloys

Aluminum reacts rapidly and irreversibly with oxygen to form a strongly-adhering oxide film, which largely determines the electrochemical behavior in aqueous electrolytes. Macdonald, in ref. 1, has described aluminum as a passive metal, which displays an active-to-passive transition, a passive region and transpassive dissolution. The current–potential relationship can be represented schematically as in Fig. 2 and a superior battery anode should, therefore, exhibit the following characteristics: (i) a very negative activation potential, (E_{CRIT}); (ii) high discharge currents at potentials only slightly

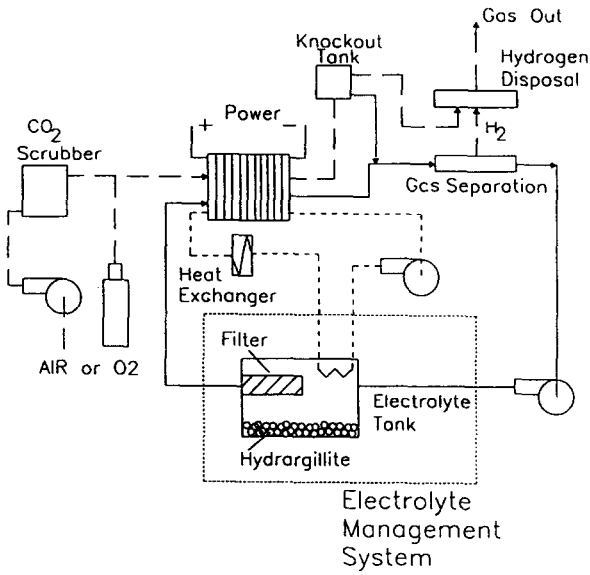

Fig. 1. Schematic representation of the aluminum/oxygen cell system. Process flow key: (——) electrolyte; (– – –) gas, and (----) coolant.

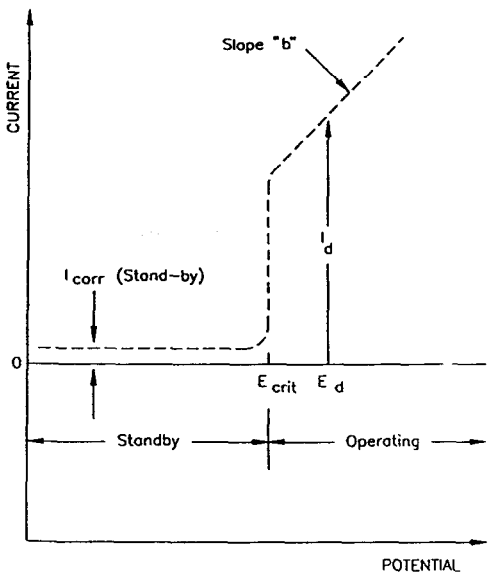

Fig. 2. Schematic representation of the current–potential relationship for aluminum in alkaline solutions.

anodic to the activation potential, i.e., a low value for the slope b, and (iii) a low corrosion current, (I_{CORR}), which remains low or decreases at the more anodic potentials required for dissolution.

Modification of the behavior of the oxide layer through the formation of alloys of aluminum has been extensively explored [2–6]. The incorporation of small concentrations of metals such as magnesium, calcium, zinc, gallium, indium, thallium, lead, mercury, and zinc, usually in combinations as ternary or quaternary alloys, has been effective in achieving activation (high rates of dissolution) and inhibition of corrosion.

The presence of certain impurities in the aluminum can markedly affect the electrochemical behavior. For example, the corrosion rate is particularly sensitive to the concentration of iron in the metal. Using manganese as an alloying element has been shown to reduce the rate of corrosion of primary aluminum (99.9% purity), which contains high levels of iron [7]. Typically alloy fabrication has used metal of higher purity, e.g., 99.995% and 99.999%.

The transition from fabrication at the laboratory-scale (bookmold ingots of weight approximately 3–5 lb) to the pilot-scale (150–250 lb ingots) is not always readily achieved. The electrochemical performance of the large ingot material can be variable and often is inferior to that of the bookmold material. That the fabrication 'practice' and thermomechanical processing is important is illustrated by the data presented in Table 1 [8]. This shows the electrochemical performance of an indium–manganese–magnesium alloy, prepared as a 150 lb ingot by direct chill casting and processed in sections to give different grain structures and microstructures (Fig. 3). For example, using the process IC, i.e., cooling slowly from the solutionizing temperature and only cold-working (cold-rolling) the alloy, will lead to an unrecrystallized structure with some precipitation of the alloying elements.

In the recent program to develop a power source for an unmanned underwater vehicle [9], emphasis has been upon mission life or the range achieved by the vehicle. It was then essential to identify an alloy with a low rate of corrosion in order to maximize the utilization of the metal fuel. An added advantage was that the hydrogen gas handling requirements within the system are minimized. The polarization characteristics remained important, as well as realizing a uniform, 'smooth' surface as dissolution proceeded.

The electrochemical characteristics of three candidate alloys are given in Table 2, show the dependence of the anode potential and corrosion-current density upon the external load. The percent utilization realized with these alloys is given in Table 3, together with data for pure aluminum and earlier alloy materials. The target

TABLE 1

Electrochemical behavior of an In–Mg–Mn alloy: effects of thermomechanical processing

Process	Open circuit		100 mA/cm²		200 mA/cm²		300 mA/cm²		400 mA/cm²	
	Potl.	Corr.	Potl.	Corr.	Potl.	Corr.	Potl.	Corr.	Potl.	Corr.
From process 1A[a]	−1.72	51.0	−1.70	35.0	−1.71	70.0	−1.66	58.5	−1.60	65.0
From process 1B[a]	−1.77	38.1	−1.74	69.0	−1.56	20.0	−1.41	22.0	−1.27	10.0
From process 1C[a]	−1.75	27.7	−1.67	31.9	−1.50	20.6	−1.38	17.5	−1.25	14.0
From process 2[a]	−1.76	30.4	−1.71	41.0	−1.69	47.4	−1.65	58.0	−1.60	60.9

[a]As in Fig. 3.
Electrolyte: 5 M KOH, 60 °C.
Potential: Volts vs. Hg/HgO reference electrode.
Corrosion: Expressed as a current density, mA/cm².

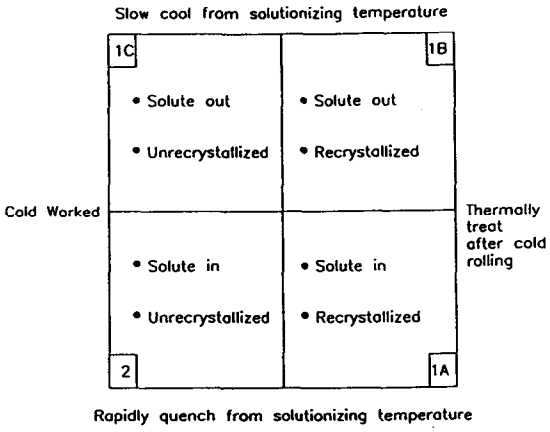

Fig. 3. Matrix to show the four types of structures resulting from the processing variations.

TABLE 2

Electrochemical performance of selected alloys

Alloy	7 mA/cm^2		25 mA/cm^2		75 mA/cm^2		125 mA/cm^2		175 mA/cm^2	
	Potl.	Corr.	Potl.	Corr.	Potl.	Corr.	Potl.	Corr.	Potl.	Corr.
ERC-2	−1.78	4.8	−1.62	2.4	−1.47	2.7	−1.42	2.25	−1.39	1.25
ERC-3	−1.77	3.5	−1.71	1.3	−1.63	0.5	−1.35	2.0		
ERC-4	−1.76	3.0	−1.58	0.2	−1.57	0.1	−1.52	0.8	−1.49	0.1

Electrolyte: 4 M KOH containing 1.5 M dissolved aluminum, 50 °C.
Electrode area: 6.45 cm^2.
Potential: Volts vs. Hg/HgO reference electrode.
Corrosion: Expressed as a current density, mA/cm^2.

levels of performance are also shown in the Table and are based upon a corrosion-current density of 5 mA/cm^2 or less over the operating range of current densities.

The alloy materials were fabricated as large ingots by conventional industry practice, although the data shown in Table 2 were obtained in laboratory-scale cells. Alloy ERC-4 is clearly superior, meeting utilization requirements while maintaining acceptable polarization behavior. Alloys ERC-2 and ERC-3 closely approached the utilization targets but the former material showed poor physical characteristics during dissolution/corrosion due to intergranular attack. This was particularly serious in the full-scale single-cell studies.

Development of air cathodes

The air cathode used in the recent programs to develop the aluminum/air or aluminum/oxygen battery as the power source in (i) an electric vehicle [8], and (ii) an unmanned, underwater vehicle is a high performance, two-layer structure. The development of air-cathode technology, involving ELTECH Research Corporation and Case Western Reserve University, has been described elsewhere [8, 9] and has led to the present electrode, which is a laminate of:

TABLE 3

Corrosion characteristics of selected aluminum alloys

Alloy	% Utilization[a]			
	5 mA/cm^2	50 mA/cm^2	100 mA/cm^2	200 mA/cm^2
High purity aluminum	0.05	31	54	76
ERC-1	12.5	56	71	81
Alcan BDW	19	72	83	92
ERC-2	43	94	97	98
ERC-3	59	98	98	
ERC-4	62.5	~99	~99	~100
Performance target	>50	>91	>95	>97.5

[a]% utilization = $\frac{\text{faradaic dissolution current (load)}}{\text{faradaic dissolution current + corrosion current}}$ %

Electrolyte: 4 M KOH containing 1.5 M dissolved aluminum.
Temperature: 50 °C.

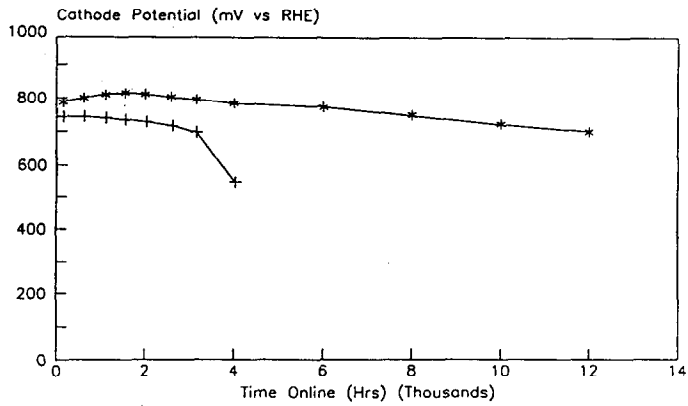

Fig. 4. Performance of polymer-modified air cathodes, constant-current operation; (*) 200 mA/cm^2 in 7.5 M KOH containing 1.0 M aluminate at 60 °C, and (+) 450 mA/cm^2 in 5.0 M KOH containing 1.0 M aluminate at 80 °C.

(i) an active layer, containing the catalyst (cobalt tetramethoxyphenylporphryn)) absorbed onto a graphitized carbon black, pyrolyzed and coated with a perfluorinated ionomer;

(ii) a gas supply layer, which is a mixture of the graphitized carbon black and Teflon, and

(iii) two nickel meshes, one on the gas side for mechanical support and the second on the electrolyte side for current distribution or collection.

This type of electrode has shown excellent extended performance under both constant-current operation (Fig. 4) and cyclic operation (Fig. 5).

For use in the unmanned, underwater vehicle, it is necessary that the transport of oxygen gas through the electrode into the electrolyte be prevented, or at least

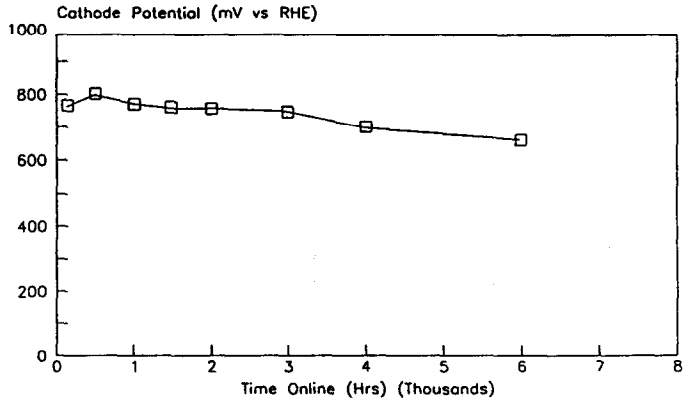

Fig. 5. Performance of polymer-modified air cathodes, cyclic operation, at 450 mA/cm^2 in 5 M KOH at 60 °C. The cell was cycled, 3 h on/3 h off. During the off-cycle, the cell remained filled with electrolyte.

TABLE 4

Electrochemical performance of the modified cathode

	Cathode potential[a] (V) vs. Hg/HgO				
	Open circuit	25 mA/cm^2	50 mA/cm^2	100 mA/cm^2	200 mA/cm^2
After 27 h at 50 mA/cm^2	+0.06	−0.07	−0.1	−0.13	−0.19
After 313 h at 50 mA/cm^2	+0.06	−0.06	−0.09	−0.12	−0.18
After 1000 h at 50 mA/cm^2	+0.07	−0.07	−0.09	−0.13	−0.21

[a]Corrected for IR contributions.
Electrolyte: 4 M KOH at 60 °C.
Gas: Oxygen, dry.
Electrode area: 14 cm^2.

minimized. A porous barrier layer was added, bonded to the nickel mesh and surface of the active layer. During operation the pores of this layer readily fill with electrolyte, providing an effective barrier to the transport of oxygen gas into the electrolyte.

The performance of the modified electrode, over the range of current densities of interest, is shown in Table 4.

Electrolyte management system

Development of the filter/crystallizer

The aluminum/air battery may operate in two basic modes, batch or steady state, depending on how one desires to treat the aluminate species generated in eqns. (1) and (2). In the batch mode, fresh electrolyte is charged into the system and operation continues until the level of dissolved aluminate reaches saturation. This situation corresponds to an end-of-charge condition; no solids are formed during batch operation. Conversely, a near constant electrolyte composition can be maintained in the steady-

state mode by promoting the crystallization of the aluminate species into an insoluble hydroxide called hydrargillite, $Al(OH)_3$ (eqn. (3)). During the cell-refueling operation, the electrolyte tank is emptied and the $Al(OH)_3$ crystals may be sent to a Hall–Heroult cell for processing back into aluminum.

The performance of a batch operation battery is electrolyte-volume limited and off-board facilities to process the supersaturated solutions of potassium aluminate would be required. Steady-state operation produces a battery with greater capacity and a more constant voltage profile versus time for a given load. By promoting the crystallization of $Al(OH)_3$ and generating KOH, the energy capacity of the battery is significantly enhanced for a given electrolyte tank volume. This fact is illustrated in Fig. 6 for a 200-liter electrolyte tank where battery capacity is plotted versus packing factor (P_f). The packing factor is a convenient way of representing filter/crystallizer performance. It may be defined as:

$$P_f = \frac{V_E + V_C}{V_C}$$

where V_E is the electrolyte volume and V_C is the volume of crystals. A packing factor of 1 corresponds to a solid mass of $Al(OH)_3$ with no entrained electrolyte. A value of 2 in the figure means that the electrolyte tank is full of a dense, paste-like slurry at the end of mission, but only 100 liters of that mass is actually $Al(OH)_3$ crystals.

Zaromb and Foust, Jr. first described operation of aluminum/air batteries with electrolyte regeneration by precipitation of $Al(OH)_3$ in 1962 [10, 11]. Since then a variety of crystallizer/separator techniques have been attempted to control the electrolyte aluminate concentration as indicated in Table 5 [12–16]. With the exception of the filtration techniques, all of these methods have been rejected for propulsion applications because of weight, volume, and/or energy considerations.

Previous studies have shown that optimization of aluminum/oxygen energy and power density requires an electrolyte management system [17, 18]. The filter/crystallizer unit patented by Coin *et al.* [19] maintains system simplicity, since only a filter and two additional valves are required. Mission duration is increased by continuously regenerating potassium hydroxide for subsequent reaction at the anode and storing

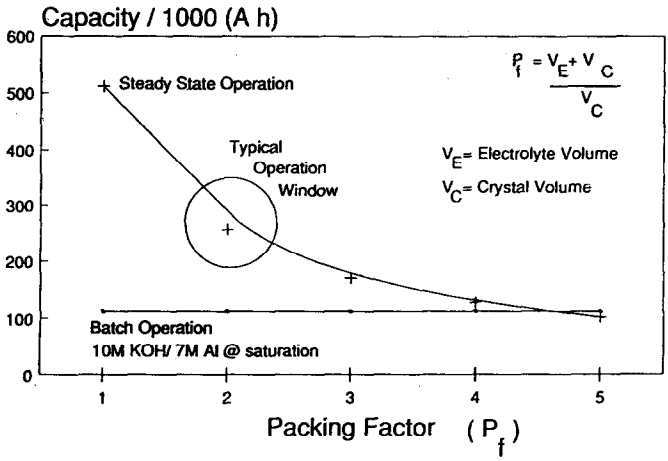

Fig. 6. Capacity for a given electrolyte volume; electrolyte tank: 200 l.

TABLE 5

Alternative solids separation techniques

Gravity settler	Wound cartridge filter
Lamella settler	Cross flow filter
Hydrocyclone	Helipump impeller fluidizer
Centrifuge	Poulos separator

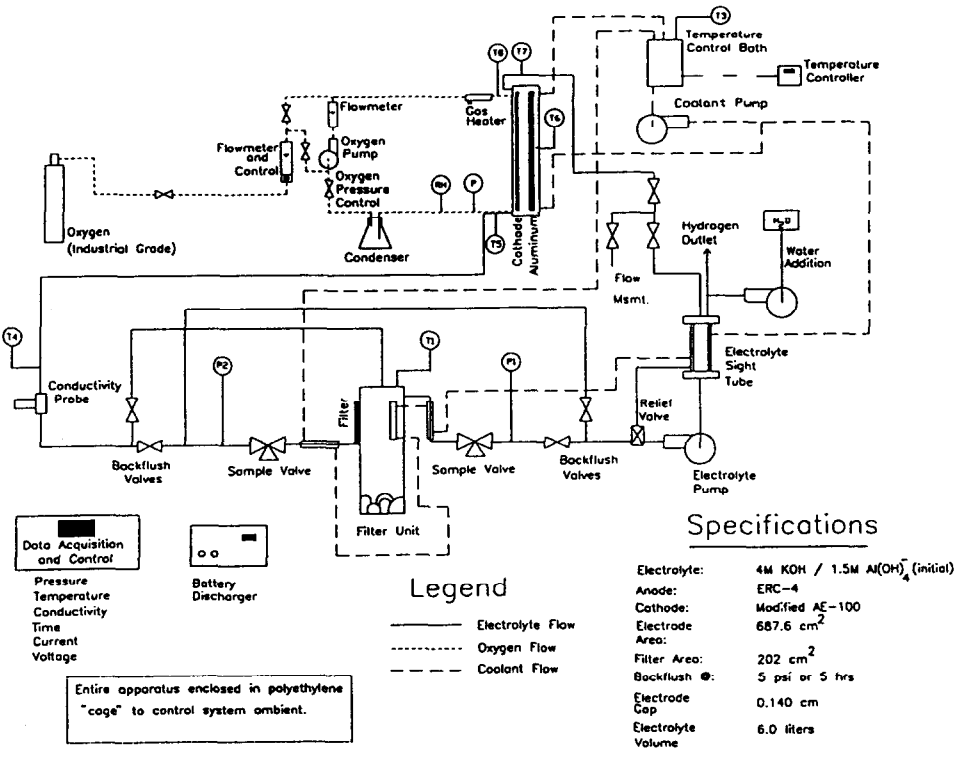

Fig. 7. Aluminum/oxygen single-cell test apparatus.

cell discharge products compactly as a crystalline hydroxide species, $Al(OH)_3$. Continuous crystallization maintains a high and nearly constant electrolyte conductivity; therefore, stack voltage remains steady throughout the discharge cycle. As the stack is discharged, a crystal cake forms and gradually increases a thickness with a subsequent increase in pressure drop across the filter. When the pressure drop reaches a predetermined level, the cake is pulsed off the filter by backflushing (flow reversal) to settle in the bottom of the tank.

Filter/crystallizer operation

Test equipment utilized to investigate the behavior of the filter/crystallizer is shown in Fig. 7. Total hydroxide concentration is kept constant by water addition and backflush cycles are produced by two-way solenoid 'backflush valves'. Figure 8 displays the results of a filter test for a power load of 40.3 A. This experiment was run in conjunction

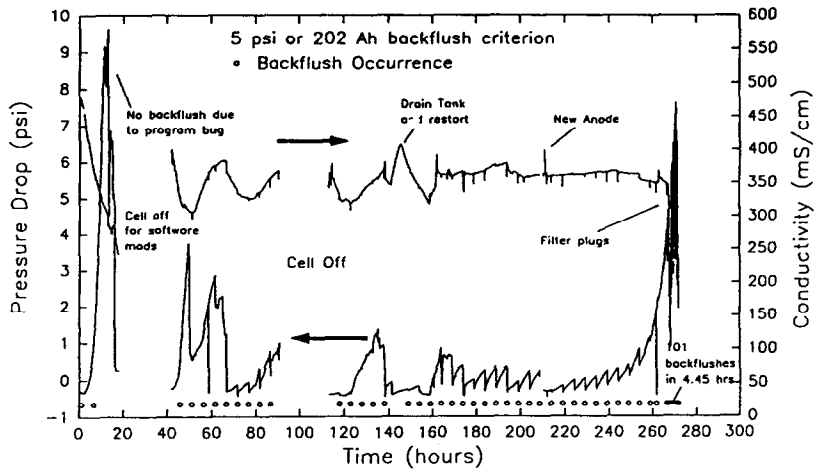

Fig. 8. Filter/crystallizer test, (50 °C, 40.32 A, 3.6 l/h; 5.8 l 4 M KOH/0.5 M Al initially; filter area: 202 cm^2, ERC-4 anode alloy).

with an aluminum half-cell driven by a power supply in which hydrogen was evolved at the nickel counter electrode. Electrolyte conductivity was continuously monitored by a Foxboro model 872 conductivity meter with an electrodeless sensor, 871EC.

Backflushes occurred at 5 psi or 202 Ah, whichever came first and, in the Fig., a hollow circle indicates a backflush. A software bug prevented the system from backflushing properly for the first 20 h. Operation began again at 40 h after the necessary software modifications were made. Despite the system upsets, the filter performed well for more than 250 h, maintaining the conductivity between 300 and 400 mS/cm. Filter lifetime depends primary on three factors: (i) the anode alloy; (ii) the filter material, and (iii) the backflush algorithm.

Aluminum/oxygen single-cell performance

Full-scale aluminum/oxygen cells (with an active electrode area of 690 cm^2) have been integrated with the filter/crystallizer unit for a series of studies. The cell featured a fixed anode with backside temperature control and a modified AE100 cathode to minimize electrolyte leakage and oxygen gas blowthrough. The anode alloy, ERC-4, was manufactured from high purity aluminum as a 150 lb ingot using conventional practice and thermomechanical processing. The experimental apparatus is that used in the filter/crystallizer studies (Fig. 7), but incorporates the aluminum/oxygen single cell. The process streams were all maintained at 50 °C with an oxygen gas flowrate of 1.75 × stoichiometry. The unreacted oxygen was recycled to the cell using a peristaltic pump.

This single cell was operated at a constant current density of 50 mA/cm^2, drawing more than 5000 Ah, during which time the cell voltage declined from 1.43 to 1.3 V (Fig. 9). This decline in the cell voltage may be attributed to the increasing interelectrode gap in this particular (fixed electrode) cell design. A movable anode prevents this ohmic voltage loss and is essential to achieve the required high energy density. The data shown represent an energy yield of 3.9 kWh/kg aluminum, which is significantly better than that obtained with earlier aluminum alloys.

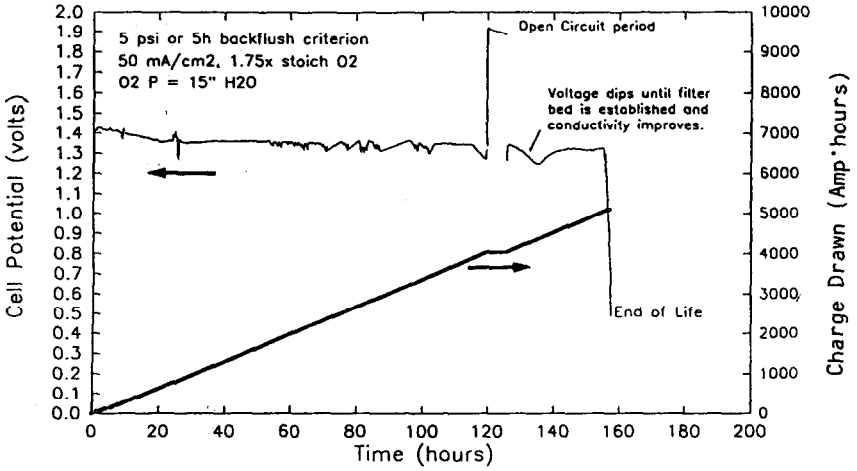

Fig. 9. Aluminum/oxygen single-cell test (50 °C, 34.38 A, 3.6 l/h, Al/O_2 single cell; 5.8 1 4 M KOH/1 M Al; ERC-4 alloy; filter area: 202 cm^2, modified AE-100).

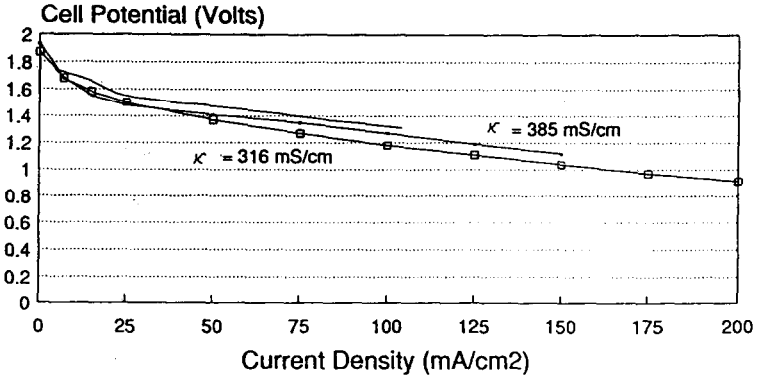

Fig. 10. Full-scale aluminum/oxygen single-cell results. Polarizations during mean power test (50 °C, 50 mA/cm^2, 1.75×recirc. O_2; 3.6 l/h, 4 M KOH/1.5 M alloy, surface area: 687.6 cm^2, modified AE-100 cathode, ERC-4 anode).

Polarization data were recorded periodically and are presented in Fig. 10 at two-time and conductivity intervals. The fact that the data obtained approach the target performance for a single cell is most promising, since, as stated above, the cell uses fixed anodes. The large decrease in cell voltage observed from open circuit to 25 mA/cm^2 is a consequence of the irreversibility of both the aluminum anode and the oxygen cathode reactions. At higher current densities the slope of the polarization curve decreases markedly, the voltage presumably being dominated by the concentration and ohmic overpotentials in the cell.

Conclusions

A brief review of the aluminum/oxygen cell and related technology has been presented. Two areas of this technology, considered to be critical to successful application

in vehicular propulsion systems, were identified. Firstly, the fabrication of high performance aluminum alloys was demonstrated, using conventional industry practice. The alloys provided the required utilization targets for the aluminum fuel in operation in a vehicle. Secondly, an effective electrolyte management system has been developed, providing the necessary control of composition and conductivity of the electrolyte as well as removing the solid by-products of the energy-producing reactions. These developments led to the integration of a single, full-size aluminum/oxygen cell with the filter/precipitator unit to give over 5000 Ah of operation, with an overall energy density of 3.9 kWh/kg aluminum.

Acknowledgements

A substantial part of this work was performed under the auspices of the Defense Advanced Research Projects Agency, Contract Number MDA-972-91-C-0040.

References

1 D.D. MacDonald, M. Urquidi-MacDonald and S. Real, Development and evaluation of anode alloys for aluminum-air batteries, *Final Rep. to Lawrence Livermore National Laboratory from ELTECH Research Corporation, Contract Number 1 806 205, Section VIIIB,* Nov. 1987.
2 J.T. Reding and J.J. Newport, *Mater. Prot., 5* (1966) 15.
3 T. Sakano, K. Toda and M. Hanoda, *Mater. Prot., 5* (1966) 45.
4 D.D. MacDonald, The metallurgy and electrochemistry of the aluminum anode, *Rep. from the Fontana Corrosion Center for ELTECH Research Corporation,* May 1984.
5 T. Valand, *Rep. to the Norwegian Defense Research Establishment, NRDE-PUBL-81/1003, 1981.*
6 E.J. Rudd and S. Lott, Aluminum-air battery development, *Final Rep. to Lawrence Livermore National Laboratory from ELTECH Research Corporation, Contract Number 1 806 205, Sections VIIIC, VIIID, and X,* Nov. 1987.
7 D.H. Scott, *Progress Rep. to Lawrence Livermore National Laboratory, UCRL-15 473,* May 1982.
8 Development of aluminum-air batteries for application in electric vehicles, *Final Rep. to Sandia National Laboratories from ELTECH Research Corporation, Contract Number SAND 91-7066,* Dec. 1990.
9 E.J. Rudd, Status of the aluminum-air battery technology, *Proc. Workshop on Structure Effects in Electrocatalysis and Oxygen Electrochemistry,* Vol. 92-11, The Electrochemical Society, Pennington, NJ, USA, 1992.
10 S. Zaromb, *J. Electrochem. Soc., 109* (1962) 1125.
11 S. Zaromb and R.A. Foust, Jr., *J. Electrochem. Soc., 109* (1962) 1191.
12 A. Maimoni, *Lawrence Livermore National Laboratory, UCRL-95 924,* 1987.
13 A. Maimoni, *Lawrence Livermore National Laboratory, UCRL-53 843,* Mar. 1988.
14 A. Maimoni, *Lawrence Livermore National Laboratory, UCRL-95 923,* Jan. 1987.
15 T.G. Swansiger and C. Misra, *Alcoa Labs, Final Rep. under Subcontract No. 57 24 709, available as UCRL-15 503,* (1982).
16 M. Balasko, R.J. Adler, R.V. Edwards and S.B. Adler, *AIChE Symp. Ser., 83* (1987) 112.
17 D.W. Gibbons, M.J. Niksa and S. Sinsabaugh, *Unmanned Syst., 9* (1991) 38.
18 A. Maimoni and J.F. Cooper, *Energy Technol. Rev., Lawrence Livermore National Laboratory,* Apr. 1988, p. 9.
19 R.J. Coin, C.W. Brown, Jr. and J.M. Noscal, *US Patent No. 4 994 332* (1991).